PAPER

Experimental study of the effect of argon on the restrike characteristics of nitrogen arc

To cite this article: Ke Shao *et al* 2022 *Plasma Sources Sci. Technol.* **31** 095008

IOP Publishing Plasma Sources Science and Technology
Plasma Sources Sci. Technol. 31 (2022) 095008 (14pp) https://doi.org/10.1088/1361-6595/ac8db9

Experimental study of the effect of argon on the restrike characteristics of nitrogen arc

Ke Shao[1,2], Su-Rong Sun[1,*], Xian Meng[2], He-Ji Huang[2], Ya-Hao Hu[1,2] and Hai-Xing Wang[1,3,*]

[1] School of Astronautics, Beihang University, 100191, Beijing, People's Republic of China
[2] Institute of Mechanics, Chinese Academy of Sciences, 100190, Beijing, People's Republic of China
[3] Ningbo Institute of Technology, Beihang University, 315800, Ningbo, People's Republic of China

E-mail: ssr18@buaa.edu.cn and whx@buaa.edu.cn

Received 3 February 2022, revised 28 July 2022
Accepted for publication 30 August 2022
Published 16 September 2022

Abstract

The arc restrike process is a typical mode of operation within a direct current arc plasma torch. By using a transfer arc device with a planar anode parallel to the gas flow direction, the effect of argon addition on the disappearance of downstream old arc roots, the overall arc downstream movement process and the generation of upstream new arc roots of the nitrogen arc restrike process is experimentally investigated. The experimental results show that for pure nitrogen arc, the restrike frequency is very high and the old arc root disappears very quickly. The addition of argon will significantly decrease the temperature of the arc root and prolong the coexistence time of the old and new arc roots. This phenomenon is caused by the rapid decay of charged particle density in the nitrogen arc, because the recombination process of charged particles in the nitrogen arc is faster than that in the argon arc. The breakdown field strength at the upstream location where the new arc root occurs is calculated by combining the measurements of arc voltage, arc grayscale image and temperature. The results show that as the percentage of argon increases, the boundary layer thickness becomes thinner and the critical electric field strength required for arc breakdown decreases, leading to the generation of new arc roots more likely to occur toward the upstream location. This study improves the understanding of the effect of argon on the nitrogen arc restrike process.

Keywords: restrike mode, nitrogen arc, argon, electric field

(Some figures may appear in colour only in the online journal)

1. Introduction

The restrike mode of anode arc root plays an important role in determining the performance of direct current (DC) arc plasma torch used for spraying applications by affecting the anode erosion and plasma arc stability [1–6]. The dynamic arc root movement may be helpful to suppress the electrode ablation [7–9], since the attachment time is short enough to heat the anode material to the melting point, but also cause the instability of arc voltage and plasma jet, which in turn affects the coating quality and torch efficiency [10–14]. Therefore, the experimental study on the restrike mode of anode arc root has received extensive and sustained attention from the arc plasma researchers [15–21].

Previous experimental studies on the restrike mode mainly focused on the evolution of arc voltage waveform and the time-resolved dynamic characteristics of anode arc root obtained by high-speed camera [22–26]. Hrabovsky recorded high-speed photos of arc anode attachment and corresponding arc voltage in a time synchronous manner to study the effect of arc anode attachment on plasma jet stability [24]. By combining the high speed arc image and voltage analysis, the quantitative correlations between the thickness of cold gas boundary layer and the arc instability mode are established [25, 26], in thus way the fluctuation mode of anode arc root under different

* Authors to whom any correspondence should be addressed.

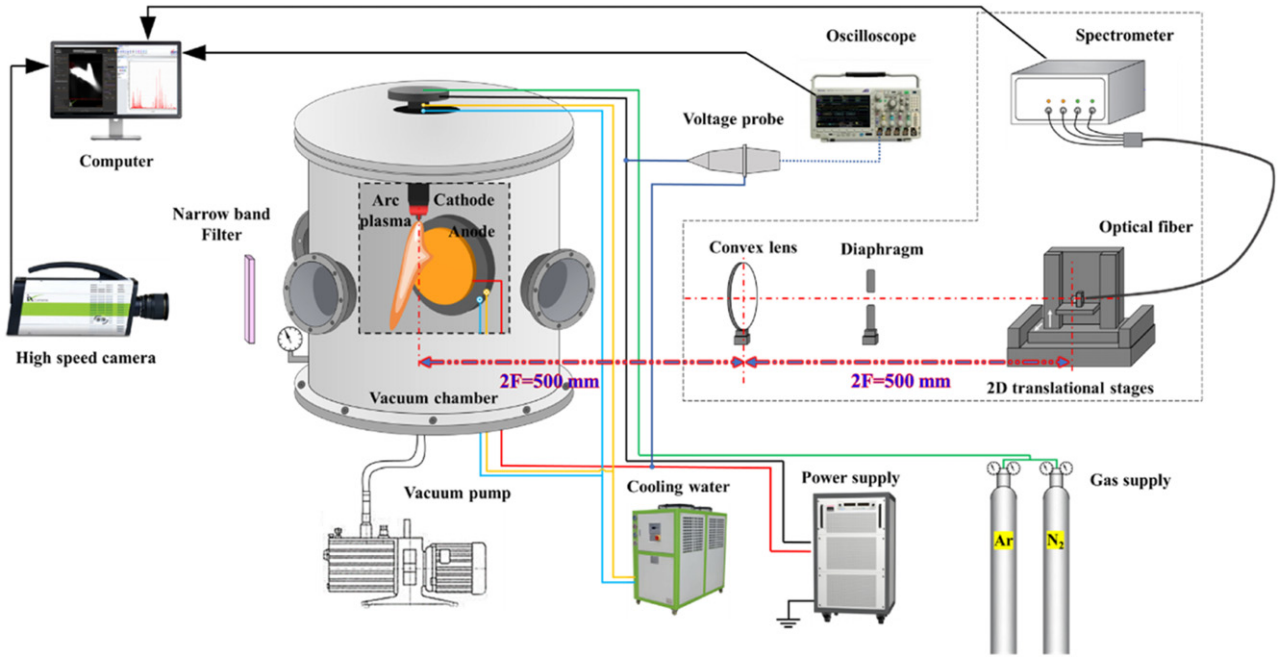

Figure 1. Schematic diagram of transferred arc device and measurement system.

conditions can be inferred by observing the influence of different parameters on the cold boundary layer thickness. The voltage waveforms could provide the information on restrike process by coupling with high-speed photography, however, the quantitative understanding of restrike process still requires the measurements of plasma parameters.

The formation of arc root restrike mode is closely related with the evolution of electric field, only when the electric field at a certain position reaches the breakdown value, the restrike mode occurs, thus the relevant parameters measurements such as temperature and electron density are critical in order to capture electric field characteristics. The measurement methods of plasma parameters in the literature mainly include Thomson scattering [27], Langmuir probe [28] and spectroscopic diagnostic technique [29–31]. The three-dimensional electron density and temperature distributions are obtained with a laser Thomson scattering system in a wall-stabilized transferred arc device with lateral gas flow, indicating that the electron overheating instabilities caused by flow instabilities are considered to be the driving mechanism for the formation of the arc restrike behavior [27]. Also the Langmuir probe measurements are performed to obtain electron temperature and electron density in the anode boundary layer of a high intensity argon arc with argon or nitrogen lateral gas flows [28]. The optical emission spectroscopy is also widely applied to investigate the variation of electron density and gas temperature [29–31]. In [31] the temperature distribution obtained by spectroscopic diagnostic technique is used to analyze the unsteadiness of DC plasma torch jets. Although the above experimental studies could provide abundant information on plasma parameters, the understanding of the restrike process requires the dynamic evolution of plasma parameter distributions. Therefore, the dynamic temperature field measurement of anode arc root restrike mode is performed in our paper to better appreciate the restrike mode.

Most of the present experimental researches on arc restrike mode used argon gas as plasma working gas [25, 32] or the main gas of argon and the cross flow gas of nitrogen [33]. As we know, different working gas has a significant influence on the arc restrike mode, especially the difference of physical properties between atomic gas and molecular gas, leading to distinct arc overall dynamic behaviors. Nitrogen gas is often used as the working gas in practical applications due to the high enthalpy property of arc plasma. Mavier *et al* investigated the restrike mode of nitrogen plasma torch, focusing on the influence of the amplitude modulation of the DC on arc motion [34]. However, the atomic gas such as argon is often added to nitrogen arc due to the instability and the nature of nitrogen arc tending to ablate electrodes. There exist some experimental and numerical literature studying Ar–N_2 arc properties in the arc plasma torch [35–38]. It is found that the addition of atomic Ar gas can significantly increase the attachment range of molecular gas N_2 arc root in plasma torch, change the arc restrike mode and improve the stability of the plasma torch jet. Therefore, the effect of argon on the complete restrike process including the generation, movement and extinction of anode arc root of nitrogen arc needs further research, which has been performed in our study.

In this paper, the experimental device with a rod-shaped cathode and a flat plate anode parallel to the axis of cathode is used to reproduce the cross gas flow in DC arc plasma torch, and the advantage of this setup is directly to observe the dynamic behavior of anode arc root. The emission spectroscopy method is used to realize the dynamic temperature field measurement. The details about the experimental setup are given in section 2. In section 3, the influence of argon gas ratio on the disappearance of downstream old arc roots,

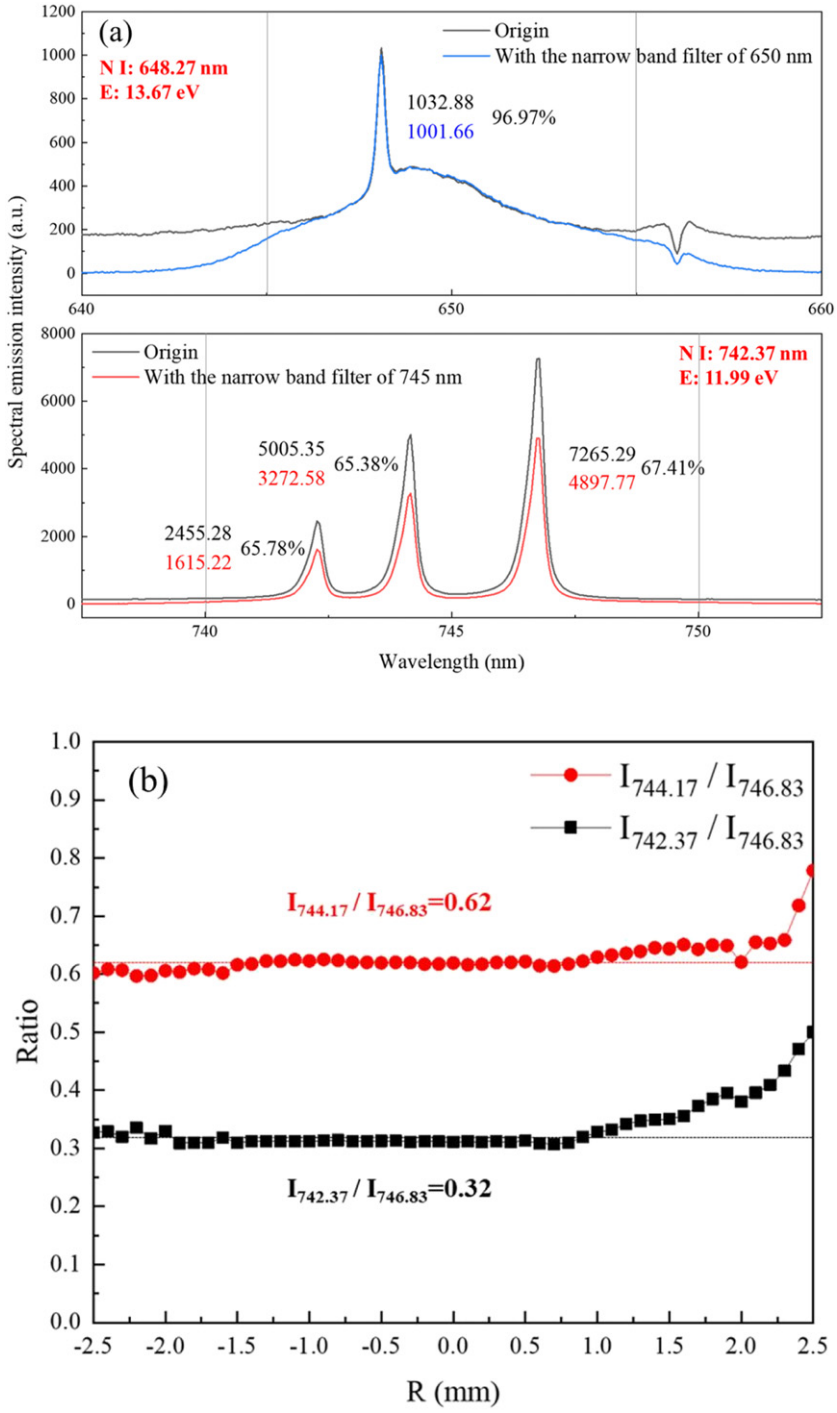

Figure 2. (a) Emission intensity at the wavelengths of 648.27 nm and 742.37 nm with or without filter, (b) ratio of emission intensity at the wavelengths of 742.37 nm, 744.17 nm and 746.83 nm.

the arc root downstream movement process and the generation of upstream new arc roots of the nitrogen arc restrike process is experimentally investigated in detail, which has never been done before. The differences between the restrike characteristics under different Ar–N_2 gas ratios are presented and explained in terms of electrical signals, high-speed images and dynamic temperature distributions, providing a basis for regulating the arc root dynamic behavior of argon–nitrogen plasma arc. Moreover, the breakdown electric field under different Ar–N_2 ratios is calculated to better understand the generation of new arc root. Finally, the conclusion is given.

2. Experimental setup

The transferred arc device and measurement system used in this study is shown in figure 1 and similar to that described in our previous paper [32]. An atmospheric pressure DC transferred arc is generated between a tungsten cathode with a

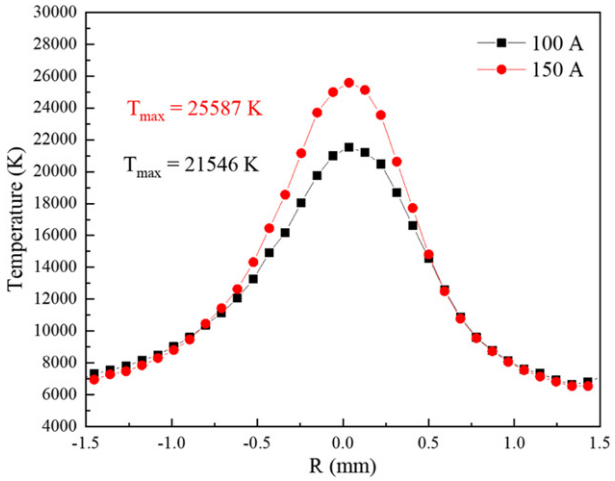

Figure 3. Temperature distribution at the axis of 0.5 mm below the cathode of the free-burning nitrogen arc (electrode gap 5 mm, flow rate 10 slm).

diameter of 5 mm and a copper anode which is parallel to the cathode axis, the distance of the anode and the cathode axis is set to 3 mm. The working gas is nitrogen and argon–nitrogen mixture, and the gas flow rate is adjusted from 5 slm to 30 slm. The arc current adjustment range is 40–160 A.

A monochromatic high-speed camera (i-SPEED 513) with a frame rate of 50 000 fps and an exposure time of 1 μs is used to observe the arc dynamic behavior. The arc voltage is obtained by measuring the voltages between the electrodes with a voltage probe (Textronix TPP0500B) and a digital oscilloscope (Textronix MDO3034). The voltage probe is connected to the power supply output, as shown in figure 1. The temperature field measurement system consists of a high-speed camera, two narrow band filters at the wavelengths of 650 nm and 745 nm with band width of 10 nm, a four-channel spectrometer (AvaSpec-ULS4096CL) that is used to record the emission intensity distributions at these two wavelengths of the arc. Since the band width of the narrow band filters used in the study is 10 nm, there are three very close nitrogen atomic spectral lines near 745 nm as shown in figure 2(a), thus we need to verify the correlation between the emission intensity variations of these three spectral lines. The ratio results of the emission intensity of 742.37 nm to 746.83 nm and 744.17 nm to 746.83 nm are shown in figure 2(b). Since the spectral intensity at different radius positions is different, the variations of the three spectral lines ratios with emission intensities are consistent. Considering the transmittance of these three spectral lines emission intensities in the 745 nm narrow band filter, we can separate the grayscale values of spectral line 742.37 nm from the grayscale image.

The main principle of this measurement method is based on the arc image processing technology and the relative intensity ratio of two specific spectral lines. Thus, two spectral lines of nitrogen atom at the wavelengths $\lambda_1 = 648.27$ nm and $\lambda_2 = 742.37$ nm respectively are selected to calculate a reasonable temperature for nitrogen and argon–nitrogen arc. The upper energy level E_1 and E_2 are respectively taken as 13.67 eV and 11.99 eV. The measured temperatures using relative intensity method with these two spectrum lines and Boltzmann plot method are very close in the range of 10 000–15 000 K. Moreover, the measured temperature distributions based on N I and Ar I lines are also very close along the cathode axis, and the maximum difference is less than 10%, so these two selected lines are reasonable for the temperature measurement. First, the calibration process is performed by using the free-burning nitrogen arc. The radial distributions of emission intensity of N I 648.27 nm and N I 742.37 nm are obtained by scanning the spectrum along the radial direction of the free-burning arc. Figure 3 shows the temperature distributions obtained by the spectroscopic line-ratio method at the axis of 0.5 mm below the cathode for different arc currents, the temperature magnitudes are similar to the experimental results measured by Haidar under the same current conditions [39], so this reasonable temperature results provide the basis for calibration and further temperature calculation in present experimental setup.

The arc images are taken by the high-speed camera with two narrow-band filters at center wavelengths of 650 nm and 745 nm respectively. Next, the function relationship between gray value and emission intensity is established by calibrating the emission intensity of the two spectrum lines with the gray value at the corresponding position in the images respectively. Therefore, the gray value recorded by the high-speed camera with different narrow band filters can be converted to the two-dimensional temperature distribution of free-burning arc by extending the function relationship to the full arc images.

Then the temperature measurement is conducted for the restrike process of arc. The gray images of arc restrike process are recorded by the high-speed camera with two narrow-band filters under the same shooting conditions. Thus the two-dimensional temperature distribution of the arc restrike mode is obtained through the same fitting formula and calculation process. More detailed descriptions can be found in [32, 40].

This temperature measurement method is based on the local thermal equilibrium assumption, which is reasonable for the arc column temperature, and provides a kind of excitation temperature in the arc fringe where the deviations from thermal equilibrium could occur. Due to the non-axisymmetric characteristic of planar anode DC arc, the Abel-inversion transformation cannot be used to obtain the local emission coefficient by spatially reconstructing the collected light intensity information. So the error of temperature measurement mainly comes from using the emission intensity superimposed along the line of sight instead of the real local emission coefficient after the spatial reconstruction by Abel-inversion. This error could also be added to the errors involved in the calibration process of emission intensity and the image matching process. The measured values along the line of sight are between the maximum and the average arc temperature, limiting its accuracy. Moreover, since the band width of the narrow band filter used in the experiment is 10 nm, the background radiation in the spectral emission intensity could also affect the accuracy of measured temperature. The H_α line in the emission intensity shown in figure 2(a) indicates the presence of water vapor in the plasma, which may affect the measured temperature. However, the effect of water vapor on the temperature is relatively

small due to the little amount of water vapor in the experiment. Finally, by comparing with the radial experimental temperature distribution at the distance of 0.5 mm below the cathode tip for 100 A nitrogen arc in [39], the maximum error is about 20% in the arc fringe region, so our measured temperature is acceptable although there exist some errors in the temperature measurement process.

3. Experimental results and discussion

3.1. Effects of argon–nitrogen ratio on the disappearing process of old arc roots

In this section we first present one complete restrike process of nitrogen arc from new arc ignition to old arc decay. Figure 4 shows the time evolution of nitrogen arc restrike process in one period at the current of 100 A and gas flow rate of 10 slm. The original old arc root is labeled with R_1 and new arc root is indicated with the symbol R_2 in the restrike process. In order to capture the fringe of arc attachment, the high-speed images are overexposed.

It is seen from figure 4 that a restrike cycle of nitrogen arc is about 0.82 ms. When a new breakdown occurs in the upstream, the upstream new arc root grows up, the downstream old arc root rapidly disappears within 0.04 ms, which indicates that there is no significant current commutation phase in the nitrogen arc restrike process. However, in our previous paper [32], it is found that the coexistence time of old and new arc roots is much longer, about 1 ms, during the argon arc restrike process. This discrepancy of old and new arc root evolution time between nitrogen and argon arcs is mainly related to the decay of charged particles densities and the drop of heavy-particle temperature. As pointed out in [41], in the post-discharge stage, the electron temperature and electric field suddenly drop, and the densities of charged particles also decay fast, while the gas temperature decreases relatively slowly.

The time and spatial evolution of arc temperature distributions at the current of 100 A and total gas flow rate of 10 slm is measured by the spectrum-image method, and exhibited in figure 5 for different Ar–N_2 ratios. The time $t = 0$ corresponds to the moment just before the occurrence of new breakdown, and the temperature evolution distributions are shown within the time of 0.06 ms.

In the case of pure nitrogen arc, the maximum arc temperature near the cathode region reaches 22 000 K. Moreover, the anode arc root is constricted and has large current density, thus its temperature is also very high and similar to the maximum temperature of the cathode arc column. Upon increasing the proportion of argon gas, the maximum temperature of arc obviously decreases. This is because the addition of argon weakens the thermal pinch effect as a consequence of lower specific heat of argon, reducing the constriction of arc column and further leading to the lower maximum arc temperature [42]. When the proportion of argon reaches 80%, the maximum temperature drops to about 18 000 K. The high temperature zone of cathode jet is shortened, and the whole arc column is more diffuse with the increase of the proportion of Ar. Under the condition of pure nitrogen arc, the temperature of anode arc root has been maintained at a high level without obvious decrease during the downstream movement, while in the case of large argon proportion, the diameter of arc root increases and the arc root attachment range becomes wide in the development stage along the anode surface, thus the temperature of anode arc root decreases gradually. Based on the temperature distributions, the process of arc root generation and disappearance also can be clearly observed. With the addition of argon gas, the disappearance time of old arc root obviously becomes long, elongating the coexistence time of old and new arc roots.

The mechanism of the downstream old arc root disappearance under different Ar–N_2 ratios is discussed and analyzed below. As expected, the number densities of charged particles and the temperature at the downstream arc root position rapidly decrease, thus the arc conductive channel at the downstream position cannot be maintained. The recombination reaction processes of charged particles are responsible for the decay of species densities, thus the dominant recombination reactions are respectively analyzed for pure argon arc and nitrogen arc. The main recombination reactions are as follows in argon arc:

$$\mathrm{Ar^+ + e + e \rightarrow Ar + e}$$

$$\mathrm{Ar^+ + Ar + e \rightarrow Ar + Ar}$$

$$\mathrm{Ar_2^+ + e \rightarrow Ar + Ar*}$$

The dissociative recombination reaction of argon molecular ions includes the recombination processes to ground state, 4s excited state and higher electronic states of argon atoms. Therefore, the summed rate constant of dissociative recombination processes of argon molecular ions is exhibited in figure 6. As the heavy-species temperature decreases with time, the argon atomic ions are converted to molecular ions, the recombination reaction process gradually becomes the dissociative recombination of argon molecular ions [41]. The dissociative recombination rate constant of argon molecular ions is obtained from literature [43–47], the electron impact three-body recombination rate constant is given in references [44, 48], and the rate constant of three-body recombination caused by heavy-species impact is extracted from reference [48].

For pure nitrogen arc, the key recombination reactions are:

$$\mathrm{N^+ + e + e \rightarrow N + \mathit{e}}$$

$$\mathrm{N^+ + N + e \rightarrow N + N}$$

$$\mathrm{N_2^+ + e \rightarrow N + N}$$

The rate constants of dissociative recombination of nitrogen molecular ions and three-body recombination due to the electron and heavy-species impact are obtained from reference [49]. Figure 6 exhibits the variation of these different recombination rate constants as a function of temperature. As shown in the figure 5, the measured arc root temperature is larger than 5000 K under different Ar–N_2 ratios. In this temperature range, from the figure 6, it is seen that the three-body recombination reactions rate constants of charged particles in

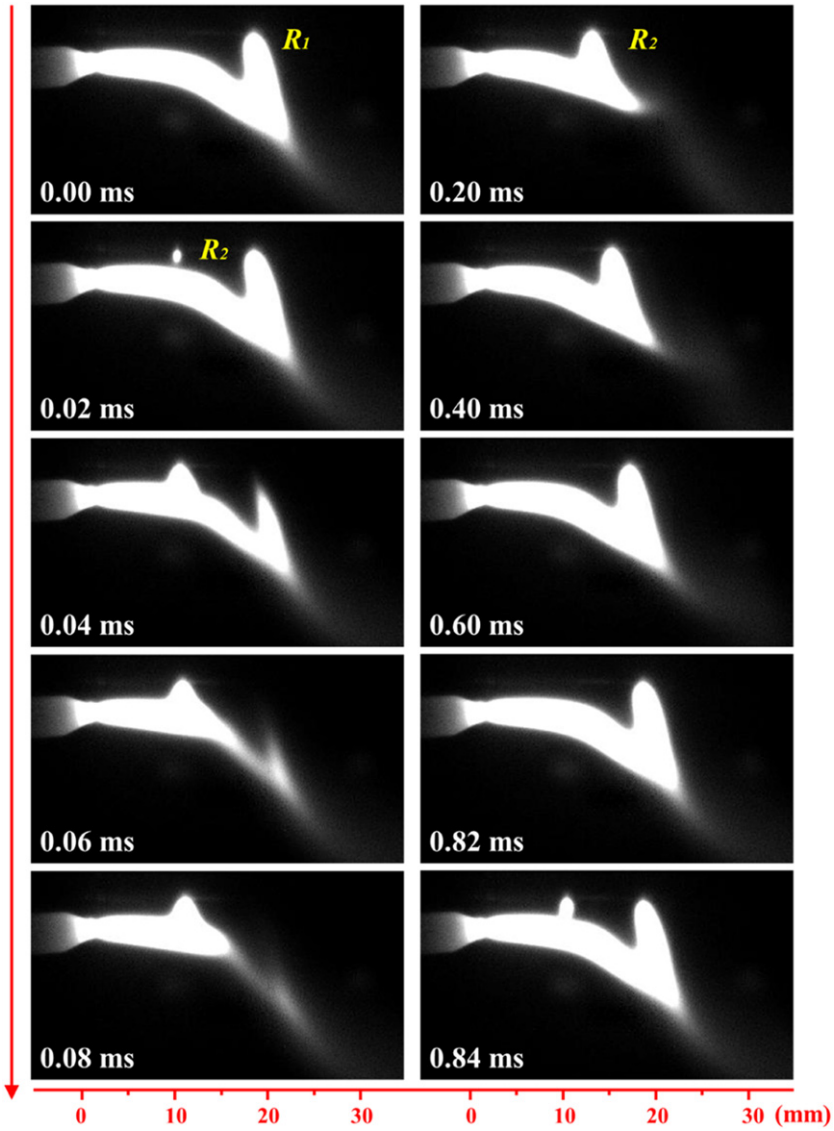

Figure 4. Successive CCD images of arc movement for the case of arc current of 100 A and gas flow rate of 10 slm. R_1 and R_2 respectively denote old and new arc attachment positions.

nitrogen plasma are significantly higher than those recombination rate constants of argon plasma, resulting in the faster loss of charged particles densities and further rapid disappearance of old arc root in nitrogen arc.

The drop of heavy-species temperature is caused by the convective and conductive loss terms in the energy equation, which is also the reason for the disappearance of downstream old arc root. In nitrogen plasma, the arc column near the anode is more constricted, the temperature is higher as shown in figure 5, and the temperature gradient is also larger. As exhibited in references [50, 51], the flow velocity in nitrogen arc is also much higher than that in argon arc. Therefore, the strong conductive and convective cooling loss of heavy-species temperature in nitrogen arc is faster, and the temperature drops more rapidly.

Due to the above two reasons, the charged particles density and temperature decay rapidly in nitrogen arc. Therefore, when the new arc root is generated upstream, the existence time of downstream old arc root is shorter than that of argon old arc root, and there is no obvious commutation time between new and old nitrogen arc roots. However, when the new breakdown occurs upstream in argon arc, the downstream old arc root can exist for a longer time and there is an obvious current commutation stage.

3.2. Effects of argon–nitrogen ratio on the arc movement characteristics during restrike process

The argon–nitrogen ratio not only affects the extinction stage of old arc root after upstream new breakdown occurs, but also change the arc root movement along the anode surface. In order to investigate the effect of argon–nitrogen ratio on arc movement, figure 7 shows the location and movement of arc root in a complete restrike period under different argon–nitrogen ratios when the current and total flow rate respectively keep to be 100 A and 10 slm. The electrode settings and image shooting conditions all adopt the same parameters in the experiment.

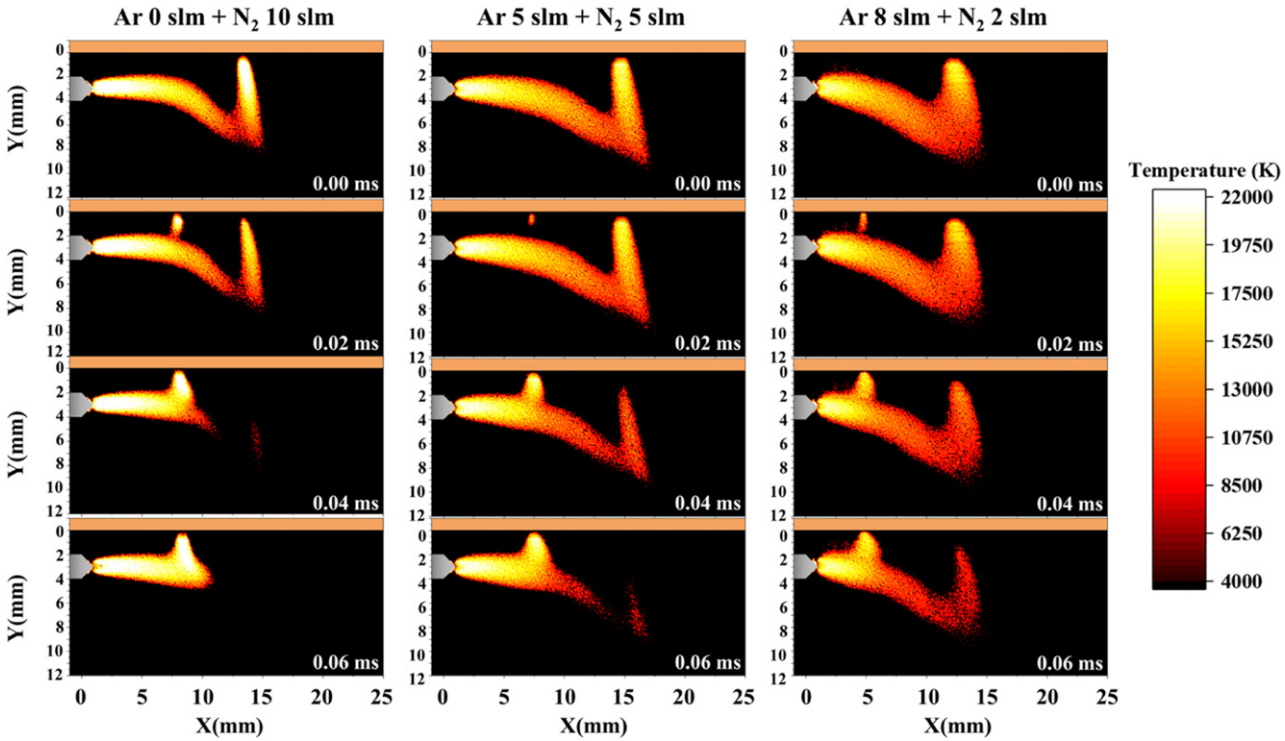

Figure 5. The arc temperature distribution during a restrike process with different Ar–N_2 gas ratios, for the case at the arc current of 100 A and total gas flow rate of 10 slm.

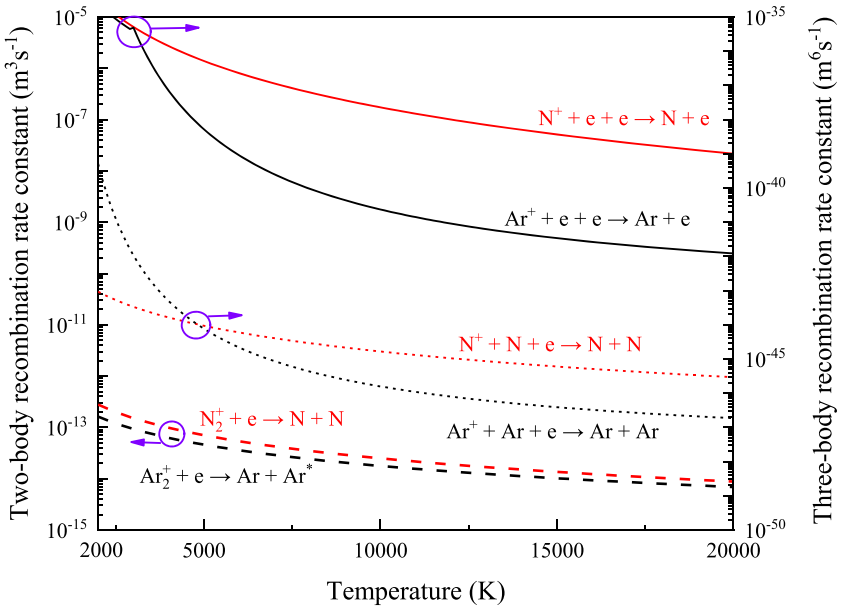

Figure 6. Variation of recombination reaction rate constants of argon and nitrogen plasma as a function of temperature.

Obviously, the cathode arc column and anode arc root are very thin in nitrogen arc. As the proportion of argon gas gradually increases, the cathode arc column and anode arc root attachment range extend. The restrike cycle time is about 0.8 ms for pure nitrogen arc, while the time required to complete a restrike process increases in argon–nitrogen mixture. When the argon proportion rises to 80%, the time for Ar–N_2 mixed gas arc to complete a cycle increases by about twice.

From the evolution of anode arc root position, it is seen that the occurrence position of new arc root of nitrogen plasma moves further downstream, which is 10.75 mm away from the cathode tip. With the addition of argon, the location of new breakdown gradually moves upward. At small argon–nitrogen ratio, the position of new arc root breakdown changes little, and the position moves upstream significantly when argon accounts for a large proportion, for example,

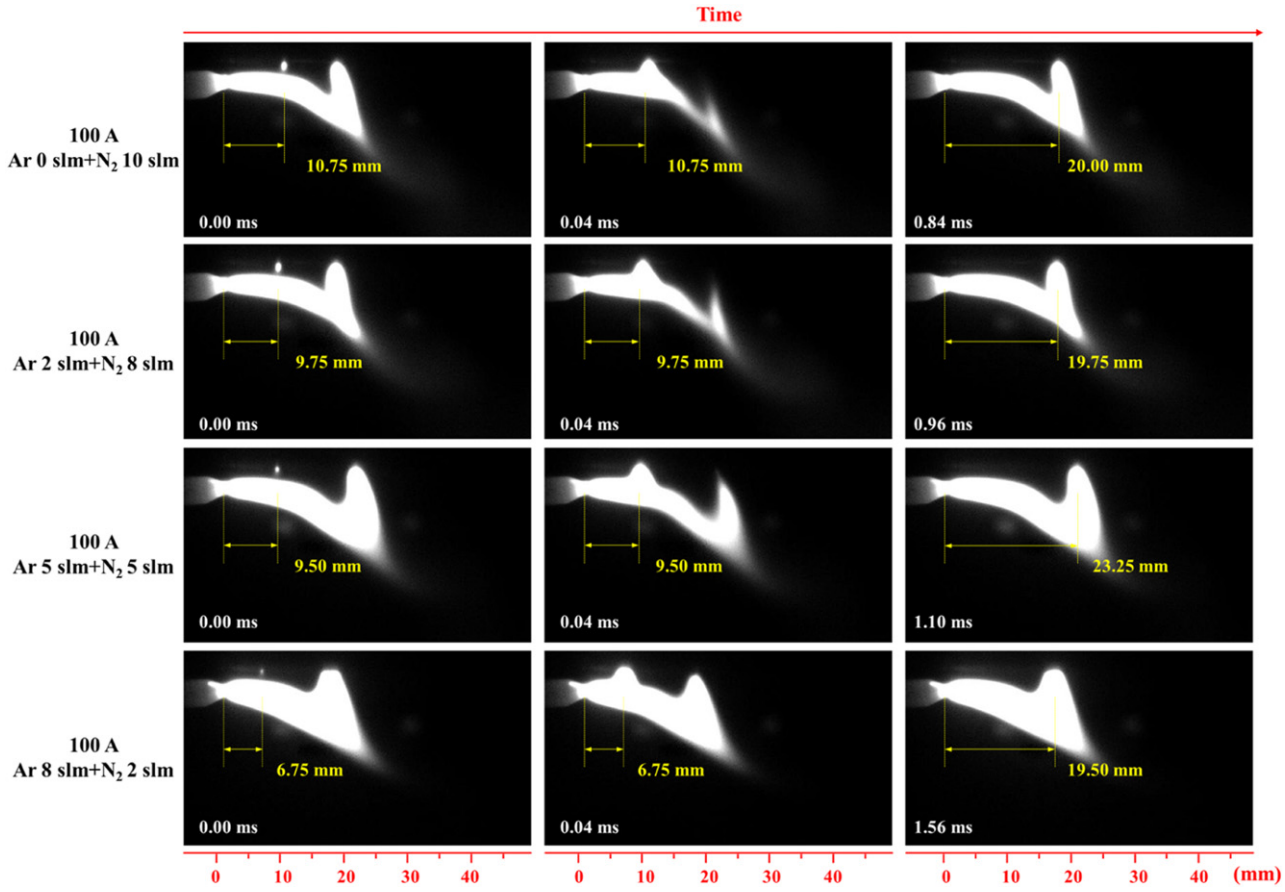

Figure 7. Frames from high-speed movie of different Ar–N_2 gas ratios in restrike mode within one period, arc current of 100 A, total flow rate of 10 slm.

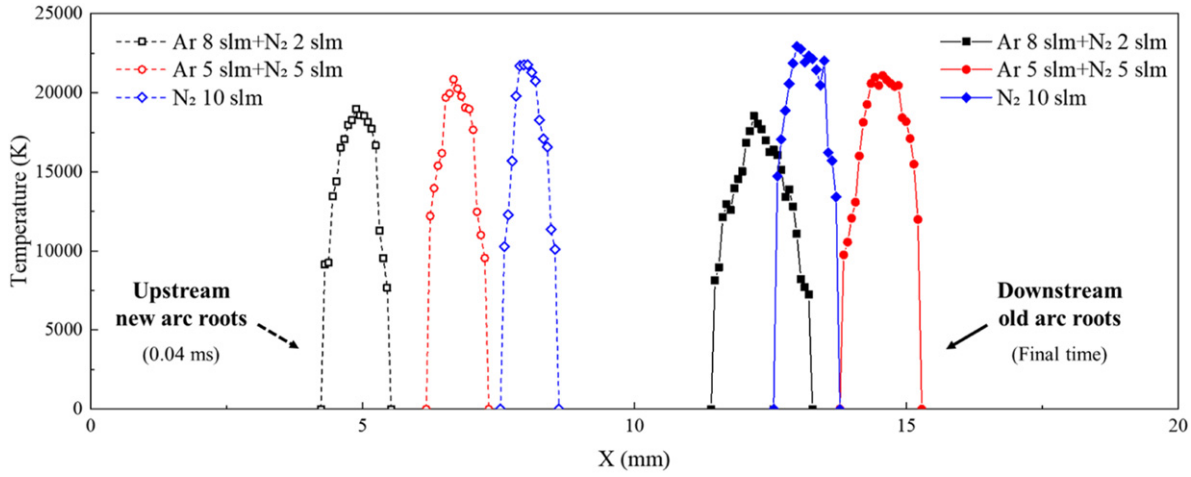

Figure 8. The arc root temperature distribution at 0.5 mm above the anode with different Ar–N_2 gas ratios, for the case with arc current of 100 A, total gas flow rate of 10 slm.

at the argon–nitrogen ratio of 8:2, the position of new arc root generation is 6.75 mm away from the cathode tip. The position of new arc root appearance is related to the electric field strength between arc column edge and anode, since the voltage difference between the maximum and minimum values in argon arc is lower than that in nitrogen arc, new arc root breakdown is likely to occur upstream in the argon arc due to the short distance of upstream arc column edge from the anode.

As shown in the figure, the change of argon–nitrogen ratio has little effect on the farthest position of anode arc root, at the argon gas flow rate of 5 slm, the anode arc root moves down furthest. According to the arc movement time and distance, we can get the arc movement velocity along the

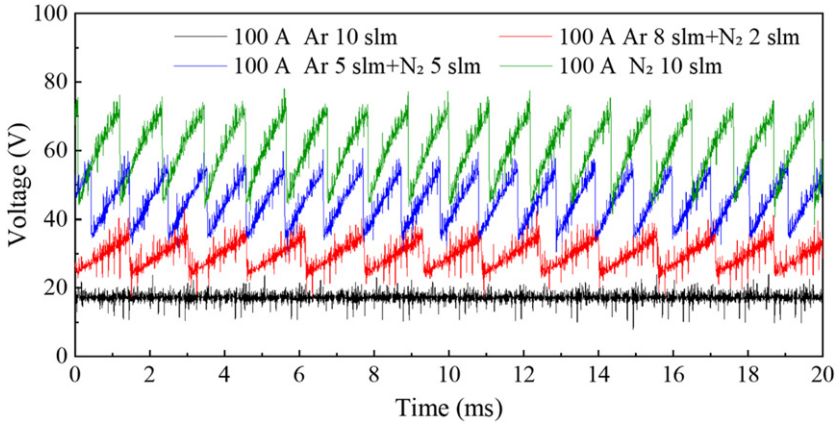

Figure 9. Arc voltage waveforms of restrike processes corresponding to different Ar–N_2 gas ratios, at an arc current of 100 A and total flow rate of 10 slm.

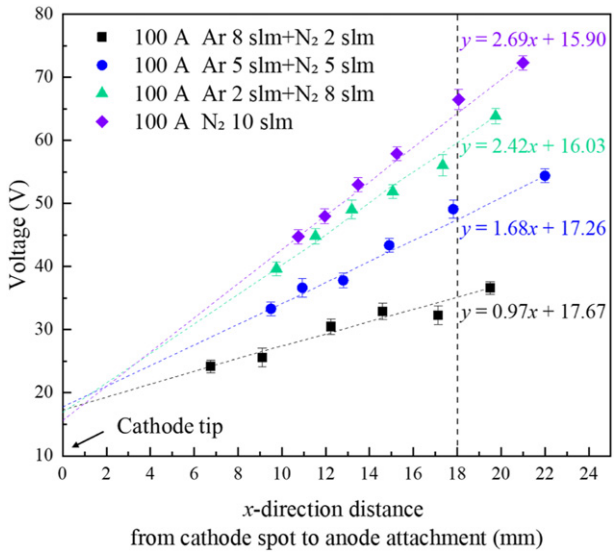

Figure 10. Variations of arc voltage with *x*-direction distance from cathode spot to anode attachment under different Ar–N_2 gas ratios at an arc current of 100 A and total flow rate of 10 slm.

anode surface. In pure nitrogen arc, the average arc movement velocity is 11.0 m s^{-1}, in argon–nitrogen mixture, the arc root velocity slows down, which respectively reaches the values of 10.42 m s^{-1} and 8.17 m s^{-1} at the Ar–N_2 ratio of 2:8 and 8:2. However, a maximum average velocity of 12.5 m s^{-1} is found at the argon–nitrogen ratio of 1:1. The anode arc root movement is determined by the combined action of gasdynamic drag and Lorentz force.

Figure 8 shows the temperature evolution during the restrike process, including new arc root temperature distribution at 0.04 ms and old arc root temperature at the distance of 0.5 mm above the anode surface. From this figure, the effect of Ar–N_2 ratio on arc temperature distributions during restrike process can be clearly seen. When the upstream new arc root just generates, the arc root temperature is high due to small arc-anode attachment range and high current density. As the arc root gradually develops and moves downstream, the arc-anode attachment range significantly increases with the rise of argon gas proportion. As the argon proportion increases from 0% to 80%, the range of the arc root temperature above 4000 K extends from 1.18 mm to 1.79 mm. However, in pure nitrogen arc, the arc root always maintains a high temperature and a small arc root diameter in the process of moving downstream. Moreover, during the downstream movement, the difference of maximum temperature under different Ar–N_2 ratios changes little. The variation of position of maximum temperature is consistent with the arc root movement shown in figure 7.

Figure 9 shows the voltage waveform of arc restrike mode under different argon–nitrogen ratios at an arc current of 100 A and total gas flow of 10 slm. The frequency of arc restrike process is the highest in pure nitrogen environment, and the arc voltage exhibits the sawtooth waveform with a large fluctuation range. As the proportion of argon increases, the frequency of arc restrike process decreases, and the amplitude of voltage fluctuation drops. In pure argon environment, the arc remains stable due to the small distance between the electrodes.

The maximum voltage corresponds to the situation that the arc root moves to the furthest downstream position, and the minimum value of arc voltage corresponds to the position where the arc breakdown occurs upstream and the new arc root becomes the main current channel. It can be clearly seen from figure 9 that both the maximum and minimum voltages decrease obviously with the rise of argon proportion. The change of arc voltage is related to two factors, i.e., the position of arc root and the type of working gas. On the one hand, with the increase of argon ratio, the position of new arc root breakdown moves upstream, so the minimum voltage definitely decreases. On the other hand, the type of working gas has an effect on the arc voltage, and the addition of argon significantly reduces the maximum arc voltage, even though the farthest position of downstream arc roots does not change significantly as discussed above.

Based on above analysis, the change of maximum arc voltage seems to have little relation with the farthest position

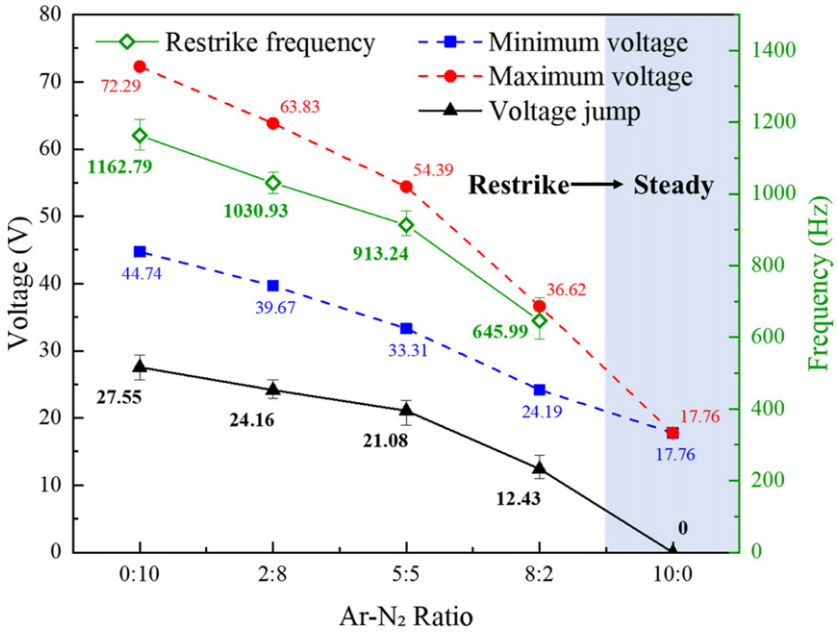

Figure 11. Variations of restrike frequency and arc voltage under different mixing gas ratios at an arc current of 100 A and total flow rate of 10 slm.

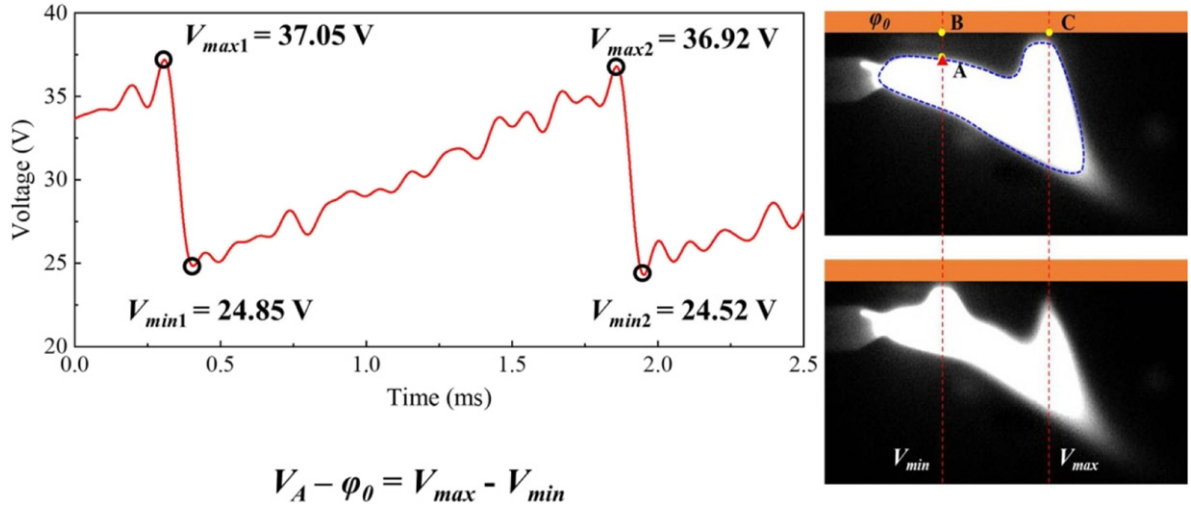

Figure 12. Schematic diagram of the breakdown voltage calculation at an arc current of 100 A and total flow rate of 10 slm, argon–nitrogen ratio of 8:2.

of downstream arc root. Combining the arc movement path in figure 7 and arc voltage results in figure 9, the variation of arc voltage with *x*-direction distance from cathode spot to anode attachment is shown in figure 10. It can be seen that the arc voltages exhibit different values, even if the distance from cathode spot to anode attachment is the same due to different gas mixing ratio. When the distance is 18 mm, the arc voltage drops from 64.3 V under pure nitrogen condition to 59.6 V at the Ar–N_2 ratio of 2:8 and 35.2 V at the Ar–N_2 ratio of 8:2. Therefore, the arc voltage difference between nitrogen arc and argon arc is seen, which is also exhibited in other experimental literatures [23, 39]. Although there is little difference in the farthest position of downstream arc root in figure 7, the maximum voltage of nitrogen arc is significantly higher than those of different argon–nitrogen gas ratios.

As seen from figure 10, the arc voltage increases linearly with the distance from cathode spot to anode attachment, and the slope represents the increase rate of arc voltage. The voltage variation rate of nitrogen arc is the fastest, so the nitrogen arc column has the highest electric field strength. The intercept of the fitting line on the *Y* axis approximates the total sheath voltage as the distance is shortened to 0. Sheath voltage indicates the potential change at the junction of arc column and electrodes, which is almost concentrated near the cathode. In this study, the sheath voltage is basically in the range of 15–17 V, and the change of working conditions has

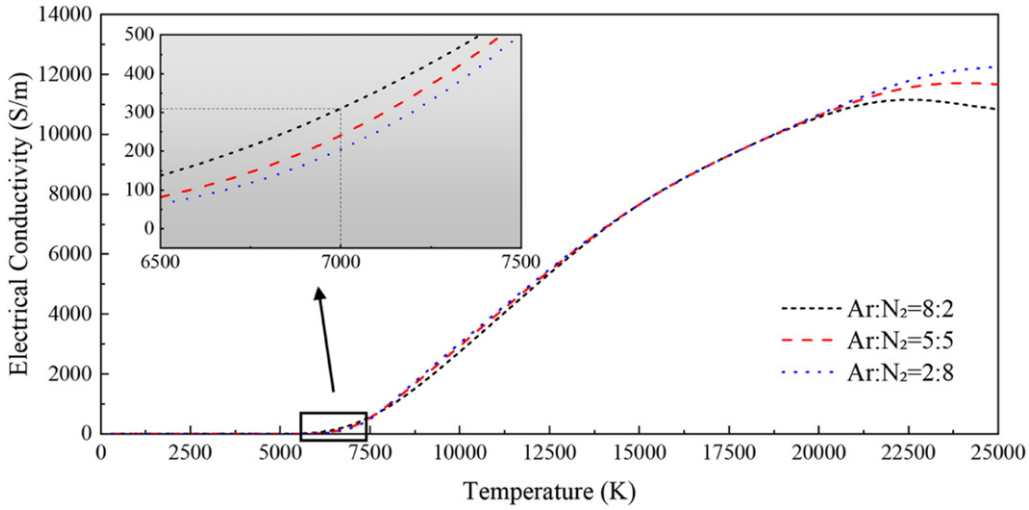

Figure 13. Variation curve of the electric conductivity with temperature under different Ar–N_2 mixing ratios.

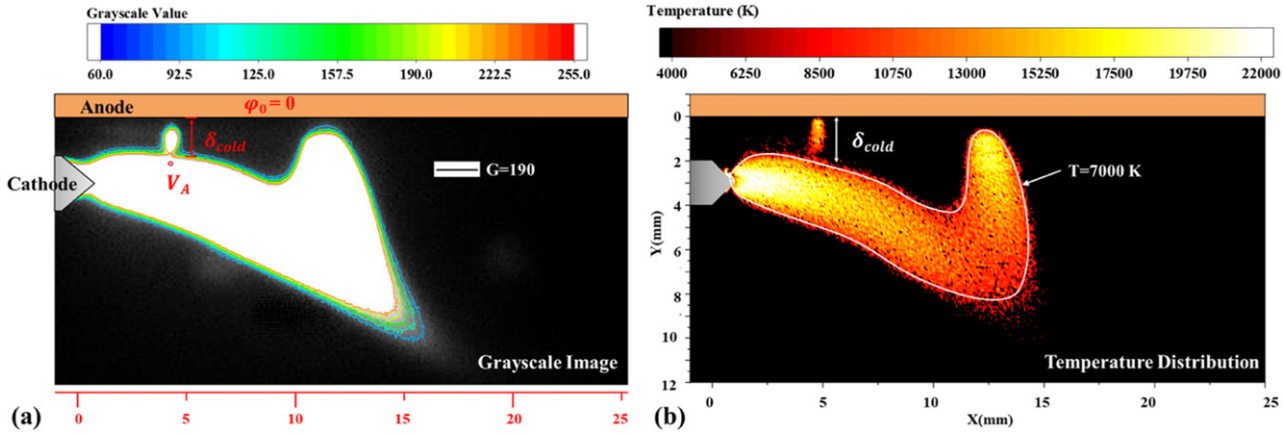

Figure 14. Schematic diagram of the cold boundary layer thickness calculation at an arc current of 100 A, total flow rate of 10 slm and argon–nitrogen ratio of 8:2.

little effect on it. This is because the change of sheath voltage is mainly controlled by cathode properties. In our previous study on plasma torch, it is found the cathode properties have an obvious influence on the sheath voltage [52], thus the change of sheath voltage is small in figure 10.

Variations of restrike frequency and amplitude of arc voltage jump with the Ar–N_2 mixing ratio are summarized in figure 11. In the pure nitrogen environment, the arc restrike frequency reaches the order of 1 kHz. The minimum voltage and maximum voltage are also the largest, thus the arc power is the highest under the same arc current and gas flow rate conditions. As the proportion of argon in the mixed gas arc increases, the arc restrike frequency, minimum voltage, maximum voltage and the voltage jump gradually decrease. When the proportion of argon increases to 80%, the voltage jump required for new re-breakdown to occur upstream is reduced by about 55%, and the restrike frequency is lowered to the order of 0.6 kHz. The pure argon arc appears to be in a steady state with a voltage of 17.76 V.

3.3. Effects of argon–nitrogen ratio on the generation of new arc roots

In this section the influence of argon–nitrogen ratio on the generation of new arc root is studied in detail. As the arc root moves downstream, the voltage drop between the upstream arc column and anode is increasing, causing the gradual increase of the electric field strength at the upstream positions. Therefore, the Joule heat in the upstream boundary layer is increasing, which leads to the enhancement of the ionization process of the upstream gas, and the rise of upstream boundary layer conductivity, finally the upstream gas breakdown occurs and a new arc channel establishes. As discussed above, the addition of argon makes the occurrence of new arc root closer to the upstream position. This new arc root position corresponds to the electric field strength reaching the critical breakdown value, thus the upstream electric field strength is analyzed below.

The critical electric field strength required for re-breakdown is defined as the voltage drop divided by the cold

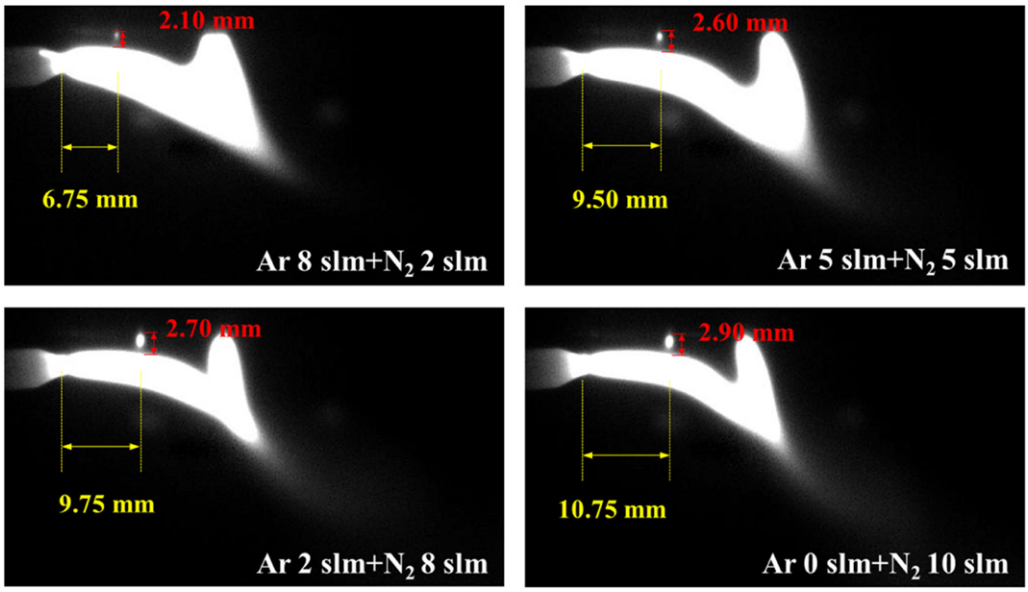

Figure 15. The cold boundary layer thickness under different mixing gas ratios at the arc current of 100 A and total gas flow rate of 10 slm.

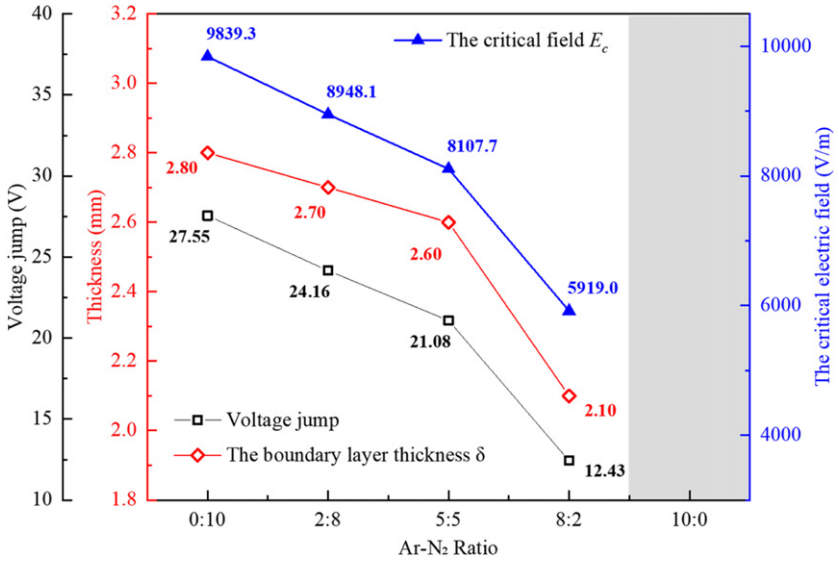

Figure 16. The cold boundary layer thickness, voltage jump and breakdown electric field strength with different mixing gas ratios at the arc current of 100 A and total gas flow rate of 10 slm.

boundary layer thickness as shown in equation (1):

$$\frac{V_{\mathrm{A}} - \varphi_0}{\delta_{\mathrm{cold}}} = E_{\mathrm{C}} \tag{1}$$

The voltage drop calculation at the breakdown position is exhibited in figure 12. The breakdown voltage of restrike process is the difference between the voltage V_{A} at the edge of arc column and anode potential φ_0 at the breakdown position. Since the anode is an equipotential surface, the voltage difference between points A and B is equal to that between points A and C, which can be calculated by the maximum voltage V_{max} corresponding to the farthest position of downstream arc root minus the minimum voltage V_{min} corresponding to the upstream new arc root generating position. So the difference between the maximum voltage and the minimum voltage is set as the breakdown voltage of restrike process.

As shown in the figure 12, taking 100 A arc current, 8 slm argon gas flow rate and 2 slm nitrogen gas flow rate as an example, the voltage drop required for breakdown can be calculated by $V_{\mathrm{max1}} - V_{\mathrm{min1}} = 12.2$ V and $V_{\mathrm{max2}} - V_{\mathrm{min2}} = 12.4$ V. Due to the repeatability of the restrike cycle, these two values of different cycles are very close and can be used to calculate the breakdown voltage.

The thickness of the cold anode boundary layer is defined by the electric conductivity lower than 300 S m^{-1} based on the reference [12]. The variation of electrical conductivity with temperature under different Ar–N_2 ratios calculated by the classical Chapman–Enskog method is shown in figure 13.

When the argon–nitrogen gas mixing ratio is 8:2, the temperature boundary is $T = 7000$ K and the corresponding grayscale boundary is $G = 190$, so the thickness of anode cold boundary layer is the distance from the arc column fringe at the temperature of 7000 K to anode surface at the position of upstream new arc occurrence, i.e., δ_{cold} as shown in figure 14. Under the other two mixing gas conditions, the temperature values corresponding to the electric conductivity 300 S m^{-1} are respectively 7140 K and 7220 K. Therefore, the cold boundary layer thickness at the breakdown position also can be determined from the corresponding temperature boundaries.

According to the above calculation method, the results of cold boundary layer thickness under different argon–nitrogen mixing ratios are shown in figure 15. The addition of argon reduces the thickness of the cold boundary layer significantly, indicating that it is more favorable for the new breakdown of the upstream arc. The thickness of cold boundary layer increases from 2.1 mm to 2.9 mm when the proportion of argon gas decreases from 80% to 0%.

Figure 16 exhibits the variations of boundary layer thickness, voltage jump and breakdown electric field strength with Ar–N_2 ratio. As the proportion of argon increases, the cold boundary layer thickness becomes thin, the amplitude of arc voltage fluctuation drops and the obtained breakdown electric field strength decreases. The critical electric field strength required for nitrogen arc breakdown reaches about 9.8 kV m^{-1}. When the proportion of argon gas flow is 80%, the breakdown electric field strength drops to about 5.9 kV m^{-1}. Since the voltage jump is small at the case of large argon proportion, the new arc breakdown occurs closer to upstream in order to reach the critical electric field strength. Although this critical breakdown electric field based on the experimental measurement data exists some extent of uncertainty, the calculation results of breakdown electric field still can provide the understanding of new arc breakdown and a reference for further theoretical analysis and numerical simulation.

4. Conclusion

In this paper, we adopt a transferred arc device with a plane anode parallel to the gas flow direction to investigate the restrike process of pure nitrogen arc and the effect of argon on the arc root disappearance, movement and generation processes. Time-resolved arc root image obtained by high-speed photography is combined with the arc voltage waveform to analyze the characteristics of restrike mode. The relative intensity method of emission spectroscopy is used to obtain the temperature distribution during the arc dynamic evolution within one cycle. Based on these experimental data, the breakdown electric field is obtained for different plasma working conditions.

The experimental results show that the restrike mode of pure nitrogen arc has a higher periodic motion frequency, faster current commutation time and larger voltage fluctuation than pure argon arc. The addition of argon can obviously prolong the co-existence time of the new and old arc roots. This phenomenon is explained from the decay of charged particles densities and heavy-species temperature drop. Based on the dynamic evolution of temperature distributions, argon can significantly reduce the arc root temperature of nitrogen arc. Meanwhile, the increase of argon proportion has an effect on the movement process of anode arc root within one restrike period. First, the arc root movement speed is slowed down as the argon ratio rises. Second, the position of new arc root generation moves closer to the upstream, and the change of argon–nitrogen ratio has little effect on the farthest position of anode arc root. The difference of arc root position is related to the gasdynamic drag force and Lorentz force. Finally, the corresponding relationship between arc voltage and anode arc root position permits us to fully understand the arc voltage variation, which is related to both the position of arc root and the type of working gas. With the increase of argon ratio, the voltage change per unit length decreases and the total arc voltage declines.

Combining the experimental results of arc voltage with the arc gray image and temperature, the breakdown field strength at the position of new arc root occurrence is calculated. The results indicate that new arc breakdown occurs more easily with the increase of argon ratio, since the critical electric field strength required for new arc root generation decreases gradually. The present results in this study are helpful to better understand the characteristics of arc restrike mode under different Ar–N_2 gas ratios, and could provide a basis for regulating the arc root dynamic behavior of argon–nitrogen plasma torch.

Acknowledgments

This work was supported by the National Natural Science Foundation of China (Grant Nos. 11735004, 12005010, 12175011), the Fundamental Research Funds for the Central Universities (YWF-22-L-1243), and Open Funding from State Key Laboratory of High-temperature Gas Dynamics, Chinese Academy of Sciences (No. 2021KF08).

Data availability statement

The data that support the findings of this study are available from the corresponding author upon reasonable request.

ORCID iDs

Su-Rong Sun https://orcid.org/0000-0002-0317-4028
He-Ji Huang https://orcid.org/0000-0002-1679-4736
Hai-Xing Wang https://orcid.org/0000-0001-7426-0946

References

[1] Pfender E 1999 *Plasma Chem. Plasma Process.* **19** 1–31
[2] Ghorui S, Sahasrabudhe S N, Murthy P S S and Das A K 2006 *Plasma Sources Sci. Technol.* **15** 689–94
[3] Vardelle A *et al* 2016 *J. Therm. Spray Technol.* **25** 1376–440
[4] Li H-P, Ostrikov K and Sun W 2018 *Phys. Rep.* **770–772** 1–45
[5] Ghorui S, Sahasrabudhe S N, Tak A K, Joshi N K, Kulkarni N V, Karmakar S, Banerjee I, Bhoraskar S V and Das A K 2006 *IEEE Trans. Plasma Sci.* **34** 121–7

[6] Li H-P, Pfender E and Chen X 2003 *J. Phys. D: Appl. Phys.* **36** 1084–96
[7] Wang C, Zhang Z, Xia W, Cui H and Xia W 2017 *Plasma Chem. Plasma Process.* **37** 371–82
[8] Wang C *et al* 2019 *Plasma Chem. Plasma Process.* **39** 402–21
[9] Nemchinsky V 2016 *IEEE Trans. Plasma Sci.* **44** 3474–8
[10] Vardelle A, Moreau C, Themelis N J and Chazelas C 2015 *Plasma Chem. Plasma Process.* **35** 491–509
[11] Saito H, Matsumoto H and Fujino T 2020 *J. Therm. Spray Technol.* **29** 333–43
[12] Moreau E, Chazelas C, Mariaux G and Vardelle A 2006 *J. Therm. Spray Technol.* **15** 524–30
[13] Pan W X, Guo Z Y, Meng X, Huang H J and Wu C K 2009 *Plasma Sources Sci. Technol.* **18** 045032
[14] Trelles J P, Heberlein J V R and Pfender E 2007 *J. Phys. D: Appl. Phys.* **40** 5937–52
[15] Wutzke S A, Pfender E and Eckert E R G 1967 *AIAA J.* **5** 707–14
[16] Krowka J, Rat V and Coudert J F 2013 *J. Phys. D: Appl. Phys.* **46** 505206
[17] Goyal V, Ravi G and Mukherjee S 2018 *Phys. Plasmas* **25** 073504
[18] Yang G and Heberlein J 2007 *Plasma Sources Sci. Technol.* **16** 529–42
[19] Sun Q *et al* 2020 *Plasma Sources Sci. Technol.* **29** 025008
[20] Tiwari N, Bhandari S and Ghorui S 2018 *Phys. Plasmas* **25** 072103
[21] Wutzke S A, Pfender E and Eckert E R G 1968 *AIAA J.* **6** 1474–82
[22] Pan W X, Meng X, Li T *et al* 2007 *Plasma Sci. Technol.* **9** 152–7
[23] Tu X, Chéron B G, Yan J H and Cen K F 2007 *J. Phys. D: Appl. Phys.* **40** 3972–9
[24] Hrabovsky M, Konrad M, Kopecky V *et al* 1999 *Ann. New York Acad. Sci.* **891** 98–105
[25] Duan Z and Heberlein J 2002 *J. Therm. Spray Technol.* **11** 44–51
[26] Noguès E *et al* 2007 *J. Therm. Spray Technol.* **16** 919–26
[27] Yang G and Heberlein J V 2007 *J. Phys. D: Appl. Phys.* **40** 5649–62
[28] Yang G, Cronin P, Heberlein J V and Pfender E 2006 *J. Phys. D: Appl. Phys.* **39** 2764–74
[29] Rajabian M, Gravelle D V and Vacquié S 2004 *Plasma Chem. Plasma Process.* **24** 261–84
[30] Li S-Z, Chen C-J, Zhang X, Zhang J and Wang Y-X 2015 *Plasma Sources Sci. Technol.* **24** 025003
[31] Zhao W, Tian K, Tang H, Liu D and Zhang G 2002 *J. Phys. D: Appl. Phys.* **35** 2815–22
[32] Shao K, Hu Y-H, Meng X, Huang H-J, Sun S-R and Wang H-X 2021 *Plasma Chem. Plasma Process.* **41** 1517–34
[33] Iwao T, Cronin P, Bendix D and Heberlein J V R 2005 *IEEE Trans. Plasma Sci.* **33** 1123–8
[34] Mavier F, Zoubian F and Rat V 2018 *J. Phys. D: Appl. Phys.* **51** 405201
[35] Selvan B, Ramachandran K, Sreekumar K P, Thiyagarajan T K and Ananthapadmanabhan P V 2009 *Plasma Sci. Technol.* **11** 679–87
[36] Selvan B, Ramachandran K, Sreekumar K P, Thiyagarajan T K and Ananthapadmanabhan P V 2009 *Vacuum* **84** 444–52
[37] Tu X, Yan J, Yu L, Cen K and Chéron B 2007 *Appl. Phys. Lett.* **91** 131501
[38] Tu X, Chéron B G, Yan J H, Yu L and Cen K F 2008 *Phys. Plasmas* **15** 053504
[39] Haidar J and Farmer A J D 1993 *J. Phys. D: Appl. Phys.* **26** 1224–9
[40] Guo H, Li P, Li H-P, Ge N and Bao C-Y 2016 *Rev. Sci. Instrum.* **87** 033502
[41] Sun S R, Kolev S, Wang H X and Bogaerts A 2017 *Plasma Sources Sci. Technol.* **26** 055017
[42] Murphy A B, Tanaka M, Tashiro S, Sato T and Lowke J J 2009 *J. Phys. D: Appl. Phys.* **42** 115205
[43] Bultel A *et al* 2002 *Phys. Rev.* E **65** 046406
[44] Sun S-R, Wang H-X, Zhu T and Murphy A B 2020 *Plasma Chem. Plasma Process.* **40** 261–82
[45] Kolev S and Bogaerts A 2015 *Plasma Sources Sci. Technol.* **24** 015025
[46] Baeva M *et al* 2012 *Phys. Rev.* E **85** 056404
[47] Zhu X-M and Pu Y-K 2010 *J. Phys. D: Appl. Phys.* **43** 015204
[48] Baeva M *et al* 2012 *Plasma Sources Sci. Technol.* **21** 055207
[49] Tanaka Y 2004 *J. Phys. D: Appl. Phys.* **37** 1190–205
[50] Tanaka M, Tashiro S, Satoh T, Murphy A B and Lowke J J 2008 *Sci. Technol. Weld. Joining* **13** 225–31
[51] Fudolig A M, Nogami H and Yagi J-i 1996 *ISIJ Int.* **36** 1222–8
[52] Sun J-H, Sun S-R, Niu C and Wang H-X 2021 *J. Phys. D: Appl. Phys.* **54** 465202